J. Fluid Mech. (2007), *vol.* 588, *pp.* 217–241.
doi:10.1017/S0022112007007458 Printed in the United Kingdom

Natural convection along a heated vertical plate immersed in a nonlinearly stratified medium: application to liquefied gas storage

M. FORESTIER AND P. HALDENWANG

Modélisation et Simulation Numérique en Mécanique et Génie des Procédés (MSNM-GP), UMR-CNRS 6181, Universités d'Aix-Marseille, EGIM/ECM

IMT/La Jetée, Technopôle de Château Gombert, 38, rue Frédéric Joliot-Curie, 13451 Marseille Cedex 20, France

(Received 10 October 2005 and in revised form 22 May 2007)

We consider free convection driven by a heated vertical plate immersed in a nonlinearly stratified medium. The plate supplies a uniform horizontal heat flux to a fluid, the bulk of which has a stable stratification, characterized by a non-uniform vertical temperature gradient. This gradient is assumed to have a typical length scale of variation, denoted Z_0, while Ψ_0 is the order of magnitude of the related heat flux that crosses the medium vertically.

We derive an analytic solution to the Boussinesq equations that extends the classical solution of Prandtl to the case of nonlinearly stratified media. This novel solution is asymptotically valid in the regime $Ra_S \gg 1$, where Ra_S denotes the Rayleigh number of nonlinear stratification, based on Z_0, Ψ_0, and the physical properties of the medium.

We then apply the new theory to the natural convection affecting the vapour phase in a liquefied pure gas tank (e.g. the cryogenic storage of hydrogen). It is assumed that the cylindrical storage tank is subject to a constant uniform heat flux on its lateral and top walls. We are interested in the vapour motion above a residual layer of liquid in equilibrium with the vapour. High-precision axisymmetric numerical computations show that the flow remains steady for a large range of parameters, and that a bulk stratification characterized by a quadratic temperature profile is undoubtedly present. The application of the theory permits a comparison of the numerical and analytic results, showing that the theory satisfactorily predicts the primary dynamical and thermal properties of the storage tank.

1. Introduction

Thermally stratified media often occur in nature. The literature on free convection – driven by various heat sources – contains numerous studies on its interaction with a stratified medium. Most analyses have focused on linear stratification, as this corresponds to a constant heat flux which crosses the medium vertically, and because this situation satisfies the conduction equation far from heat sources. However, other stratification situations arise that are not based on pure heat diffusion. The purpose of the present work is to analyse a particular case of natural convection in nonlinearly stratified medium.

The study is motivated by problems arising in energy storage. Such problems are often crucial with respect to certain new forms of energy, especially concerning their use in transport or industry. The problems become important for the cryogenic

storage of fuels such as hydrogen. The present theoretical and numerical studies are therefore motivated by the need for a better understanding of the thermal state in a cryogenic gas tank. The natural convection in such cases of industrial storage is characterized by flow patterns obtained at very high Rayleigh numbers. One can hence expect stratification of the bulk, and thin buoyancy layers (sometimes refered to as convective boundary layers, i.e. the thin region along the heated wall where the fluid motion is generated).

The idealized tank configuration we study in the second part of the paper reveals that thermal stratification is indeed achieved, and is characterized by a non-uniform vertical thermal gradient. This nonlinear stratification arises from the fact that the bulk thermal state depends on factors in addition to vertical conduction. This observation (established by the numerical simulations described later) leads us to consider the theoretical problem of a uniformly heated vertical plate immersed in a nonlinearly stratified medium. This issue is analytically solved by deriving an approximate solution, which appears as an extension of the classical solution 'mountain and valley winds in stratified air' established by Prandtl (1952). The extension thus considers a medium, the stratification of which admits a non-zero second-order vertical derivative of its temperature profile. We then apply this new theory to the practical case mentioned above. More precisely, the numerical computation of the axisymmetrical natural convection in a cylindrical container is considered, and the theoretical predictions are compared to numerical computations.

It has long been known that high-Rayleigh-number convection in an enclosure driven by a vertical wall leads to stable thermal stratification of the cavity bulk. This was observed in the numerous experimental results in Turner (1973). This feature was also evident in the numerical results of Haldenwang (1986), and more recently in numerical studies by Ravi, Henkes & Hoogendoorn (1994) on Prandtl number effects for such a thermal stratification. The establishment of such stratification is often preceded by the downward motion of a transient front that separates the recently heated upper bulk from the initial cool environment (see Baines & Turner 1969 when the heat source is composed of plumes, and Hunt, Cooper & Linden 2001 for the case of hot jets). Similar transient results are evident in the present numerical studies, provided that the Rayleigh number is chosen sufficiently high. This article nevertheless focuses on flows that have reached an overall steady state, the properties of which are related to free convection on walls immersed in a thermally stratified medium.

This problem has received substantial attention in literature, because numerous geophysical and oceanic convective flows also occur in various stratified media. The seminal analytical solution of Prandtl (1952), 'mountain and valley winds in stratified air', supplies the exact solution for natural convection along a slope that is maintained with a constant temperature excess with respect to the outer air linear stratification. A plane parallel flow is generated along the slope, exhibiting flow reversal and temperature defect, both of which have appeared much later as characteristics of convection in a stratified medium, as e.g. shown in Tanny & Cohen (1998).

The problem of a vertical wall immersed in a thermally stratified environment has also been considered in the context of certain similarity solutions that lead to a set of ordinary differential equations. In that framework, particular cases of temperature excess at the wall and stratification profiles have been investigated by Yang, Novotny & Cheng (1972). The case of an isothermal wall immersed in a particular polynomial profile of thermal stratification was solved in Kulkarni, Jacobs & Hwang (1987). The approach was extended to more general fixed wall temperatures by Henkes & Hoogendoorn (1989). A recent contribution by Tao,

Le Quéré & Xin (2004) supplied a similarity solution for prescribed linearly increasing temperatures as both wall and bulk boundary conditions. For the case of uniform heat flux, as studied in the present contribution, Jaluria & Gebhart (1974) found a theoretical similarity solution, provided that the ambient stratification varies like $z^{1/5}$, where z is the vertical (or downstream) coordinate. Sundstrom & Kimura (1996) found an analytical solution that describes the plane parallel convection occurring between two inclined parallel heated walls which create a constant stratification. The classical related problem of the unsteady buoyancy flow induced in response to a suddenly imposed plate heat flux was recently revisited by Shapiro & Fedorovich (2004*a*, *b*). Finally, note that most of those analytical or analytical/numerical steady solutions have been the subject of stability analysis (see Gill & Davey (1969), Krizhevsky, Cohen & Tanny (1996), Sundstrom & Kimura (1996), Tao *et al.* (2004)).

The present contribution endeavours to derive an analytical expression that supplies an approximate solution to the Boussinesq equations. The validity of this approach is expected to hold in the limit $Ra_S \to \infty$, where Ra_S is the Rayleigh number that characterizes the nonlinear stratification. The thermal boundary conditions at the immersed wall are of uniform-heat-flux type and any form of stable stratification is allowed in the bulk (if Ra_S is large enough). We note that the present analysis extends the Prandtl solution and the similarity solution of Jaluria & Gebhart (1974) to the general case of nonlinear stratification.

Section 2 is devoted to the analytical approach, which is intended to solve the Boussinesq equations with the boundary conditions suitable for the present problem of natural convection in a stratified medium. The 'mountain and valley winds in stratified air' solution by Prandtl (1952) is first evoked, and we show how it can provide intuition related to our analysis. We then develop the analytical approach, which takes advantage of the scale separation between horizontal and vertical variations in the buoyancy layer. Finally, we discuss the validity of this approximate solution.

Section 3 presents an analysis of a storage tank as a practical application of the theory. We first give a brief overview of the high-accuracy numerical method that we developed for solving the Boussinesq equations in a cylindrical geometry with axisymmetrical assumptions. We then report on a set of numerical data for a large range of $Ra = g\alpha\,\phi_0\,R^4/\nu\kappa\lambda$, (where the symbols are defined in § 2.1) the cavity Rayleigh number (i.e. $10^7 < Ra < 10^{12}$), where we note the thermal stratification of the bulk medium, a characteristic that allows us to apply our theory. We relate the stratification Rayleigh number (Ra_S) to the cavity Rayleigh number (Ra). Finally, the quantitative predictions resulting from the present theory are compared to the detailed numerical results. A satisfactory agreement is found for high Ra.

2. Analytical approach

2.1. *Mathematical formulation*

We consider steady flow adjacent to an infinite vertical plate, located at $x = 0$. This wall provides the stratified fluid with a uniform horizontal heat flux, ϕ_0. The fluid medium occupies the semi-infinite bi-dimensional domain

$$\Omega = \{0 < x < \infty\} \times \{-\infty < z < \infty\}. \tag{2.1}$$

The governing equations are chosen within the framework of the Boussinesq–Oberbeck approximation: the fluid has uniform density ρ_0 except for the buoyancy force. We denote as $\boldsymbol{V}$ the velocity, T the temperature, and P the pressure departure from the hydrostatic pressure related to the constant density fluid. Furthermore,

we define ν, κ, α and g, as the fluid kinematic viscosity, thermal diffusivity, thermal expansion coefficient, and gravitational acceleration, respectively. The set of governing equations is

$$\nabla \cdot \boldsymbol{V} = 0 \qquad \text{in} \quad \Omega, \tag{2.2}$$

$$\nabla \boldsymbol{V} \cdot \boldsymbol{V} = -\nabla\left(\frac{P}{\rho_0}\right) + \nu \Delta \boldsymbol{V} + \alpha g T \boldsymbol{e}_z \qquad \text{in} \quad \Omega, \tag{2.3}$$

$$\nabla T \cdot \boldsymbol{V} = \kappa \Delta T \qquad \text{in} \quad \Omega, \tag{2.4}$$

together with the boundary conditions

$$\boldsymbol{V}(x = 0, z) = 0, \quad \boldsymbol{V}(x = \infty, z) = 0, \tag{2.5}$$

$$\frac{\partial T}{\partial x}(x = 0, z) = -\frac{\phi_0}{\lambda}, \quad T(x = \infty, z) = T_s(z), \tag{2.6}$$

where λ is the thermal conductivity and $T_s(z)$ is the prescribed temperature profile in the stratified medium. $T_s(z)$ is a general function of z, the first derivative of which is assumed to be positive, while the second derivative may differ from zero, i.e. a nonlinear thermal profile in the bulk.

2.2. *The Prandtl exact solution 'mountain and valley winds'*

In 1952, L. Prandtl gave an exact solution to the problem of an infinite vertical plate immersed in a linearly stratified fluid, i.e. characterized by a uniform thermal vertical gradient in the bulk (see the discussion in Gill 1966 for possible applications in enclosures). The temperature profile prescribed far from the plate is $T(x = \infty, z) = T_s(z) = \psi_0 z/\lambda$, where ψ_0 is the vertical heat flux through the stratified bulk. The plate has a linearly varying temperature $T(x = 0, z) = \psi_0 z/\lambda + \Delta T$, which differs from that of the bulk by the uniform temperature increment ΔT. Prandtl found a solution in the form of a plane parallel flow such that

$$T(x, z) = T_s(z) + \theta(x), \tag{2.7}$$

$$\boldsymbol{V}(x, z) = V_z(x)\, \boldsymbol{e}_z, \tag{2.8}$$

with

$$\theta(x) = \theta_0 \exp\left(\frac{-x}{l_0}\right) \cos\left(\frac{x}{l_0}\right), \tag{2.9}$$

$$V_z(x) = V_0 \exp\left(\frac{-x}{l_0}\right) \sin\left(\frac{x}{l_0}\right), \tag{2.10}$$

and where

$$l_0 = \left(\frac{4\nu\kappa\lambda}{\psi_0 \alpha g}\right)^{1/4}, \tag{2.11}$$

$$\theta_0 = \Delta T, \tag{2.12}$$

$$V_0 = \frac{\kappa \psi_0}{\lambda \Delta T}\left(\frac{\alpha g \lambda^3 \Delta T^4}{\kappa \nu \psi_0^3}\right)^{1/2} \tag{2.13}$$

are respectively the boundary layer thickness, the thermal departure at the wall, and the strength of convection motion.

This exact solution is identical to the solution of the problem with prescribed thermal flux at the plate. The heat flux supplied by the plate is $-\lambda\, \mathrm{d}\theta(x = 0)/\mathrm{d}x = \lambda \Delta T/l_0$, and therefore admits a uniform value. Then, equating $\lambda \Delta T/l_0$ with ϕ_0, the

thermal departure and the convective velocity strength can be rewritten as

$$\theta_0 = \sqrt{2}\frac{\phi_0 l_0}{\lambda}\left(\frac{\alpha g \psi_0 l_0^4}{\nu\kappa\lambda^3}\right)^{-1/4} = \left(\frac{\phi_0}{\psi_0}\right)^{1/4}\left(\frac{4\nu\kappa\phi_0^3}{\lambda^3\alpha g}\right)^{1/4}, \tag{2.14}$$

$$V_0 = \sqrt{2}\frac{\kappa}{l_0}\left(\frac{\alpha g \psi_0 l_0^4}{\nu\kappa\lambda^3}\right)^{1/4}\frac{\phi_0}{\psi_0} = \left(\frac{\phi_0}{\psi_0}\right)^{3/4}\left(\frac{4\alpha g\kappa^3\phi_0}{\nu\lambda}\right)^{1/4}. \tag{2.15}$$

Our intent is to extend these expressions at fixed flux by deriving an approximate solution in the case of a nonlinearly stratified medium, i.e. with a non-constant thermal gradient $\mathrm{d}T_s(z)/\mathrm{d}z \neq \psi_0/\lambda$. This extension will appear as a simple adaptation of the quantity ψ_0 contained in (2.11) and (2.14)–(2.15).

2.3. *An approximate solution for nonlinear stratification*

We now develop an approximate analytical approach to the problem of free convection induced by uniform heating ϕ_0 along a vertical infinite plate in a medium, the stratification of which is $T_s(z)$. The vertical gradient is the non-constant quantity $T_s'(z)$ with $T_s' > 0$ (i.e. the medium is assumed to be stable). We postulate that the order of magnitude of the vertical heat flux that crosses the medium, denoted Ψ_0, is such that

$$\frac{\mathrm{d}T_s(z)}{\mathrm{d}z} = O\left(\frac{\Psi_0}{\lambda}\right). \tag{2.16}$$

Since the stratification is assumed to be nonlinear, $\mathrm{d}^2T_s(z)/\mathrm{d}z^2$ is non-zero. We denote the typical magnitude of these non-zero values as $\| \mathrm{d}^2T_s(z)/\mathrm{d}z^2 \|$. Hence, we can now define Z_0, the typical variation length of nonlinear stratification, as

$$Z_0 \equiv \frac{\Psi_0}{\lambda}\left\| \frac{\mathrm{d}^2T_s}{\mathrm{d}z^2} \right\|^{-1}. \tag{2.17}$$

Let us first comment that Z_0 tends to infinity as the stratification becomes linear. As a result, Z_0 is an additional length scale, which characterizes the deviation from linearity in the temperature profile. In what follows, Z_0 is conceived as a length scale, which is large compared with l_0, the typical thickness of the convection boundary layer.

This idea of length scale separation motivates us to introduce $\{\xi, \hat{z}\}$, a new set of dimensionless variables defined as

$$\xi(x,z) \equiv \frac{x}{Z_0\delta(\hat{z})}, \qquad \hat{z} \equiv \frac{z}{Z_0}. \tag{2.18}$$

If $\delta(\hat{z})$ is a small quantity (to be characterized later), the new variable ξ allows us to focus on the zone close to $x = 0$, where the convective boundary layer is localized, its thickness assumed to be of the order of $Z_0\delta(\hat{z})$ (with $|\,\delta\,| \ll 1$). The two original partial derivations are then expressed as

$$\frac{\partial}{\partial x} = \frac{-1}{Z_0\delta}\frac{\partial}{\partial\xi}, \qquad \frac{\partial}{\partial z} = \frac{1}{Z_0}\left(\frac{\partial}{\partial\hat{z}} - \frac{\xi}{\delta}\frac{\mathrm{d}\delta}{\mathrm{d}\hat{z}}\frac{\partial}{\partial\xi}\right). \tag{2.19}$$

In this context, all space derivatives of any quantity will keep the same dimension as the original quantity, the new space variables being dimensionless. Furthermore, to avoid introducing numerous new non-dimensional unknowns, in what follows we only make dimensionless the stratification temperature. The reason is that only the magnitudes of stratification scale and gradient are needed for constructing the forthcoming Rayleigh number of stratification. Additionally, we anticipate that any

function of $\hat{z}$ has a slow variation: for example, we postulate that $\delta' \equiv \mathrm{d}\delta/\mathrm{d}\hat{z} = O(\delta)$. We now look for an approximate solution in the mathematical framework of separation of variables. To do this we postulate that the temperature field satisfies the following form:

$$T(x, z) = \frac{\Psi_0 Z_0}{\lambda} \hat{T}_s(\hat{z}) + \theta(\xi)\tau(\hat{z}), \tag{2.20}$$

where $\theta(\xi)$ and $\tau(\hat{z})$ are two functions whose scale of variation is $O(1)$. $\hat{T}_s(\hat{z})$ is the imposed stratification profile made dimensionless for the sake of future simplification of the notation. For the vertical component of velocity, we can similarly assume the form

$$V_z(x, z) = \boldsymbol{V}(x, z) \cdot \boldsymbol{e}_z = V(\xi)\gamma(\hat{z}). \tag{2.21}$$

As for the pressure field, we similarly postulate

$$P(x, z) = -\int \alpha g \rho_0 \frac{\Psi_0 Z_0^2}{\lambda} \hat{T}_s(\hat{z})\, \mathrm{d}\hat{z} + p(\xi)\pi(\hat{z}), \tag{2.22}$$

where the first term of the right-hand side is simply the next order of the hydrostatic pressure variation in the stratified bulk. In accordance with the above assumptions, our purpose is now to convert expressions (2.20)–(2.22) into steady Boussinesq equations and to develop that system at the lowest order in δ.

We first derive V_x, the transverse component of velocity, from the incompressibility constraint. This yields

$$\frac{1}{Z_0\delta}\frac{\partial V_x}{\partial \xi} + \frac{V}{Z_0}\frac{\mathrm{d}\gamma}{\mathrm{d}\hat{z}} - \frac{\xi}{Z_0\delta}\frac{\mathrm{d}\delta}{\mathrm{d}\hat{z}}\frac{\partial V}{\partial \xi}\gamma = 0. \tag{2.23}$$

After partial integration of $\partial V_x/\partial\xi$, we get

$$V_x(\xi, \hat{z}) = u(\xi)\frac{\mathrm{d}\delta}{\mathrm{d}\hat{z}}(\hat{z})\gamma(\hat{z}) - v(\xi)\delta(\hat{z})\frac{\mathrm{d}\gamma}{\mathrm{d}\hat{z}}(\hat{z}) \tag{2.24}$$

with

$$u(\xi) = \int_0^\xi \xi \frac{\mathrm{d}V}{\mathrm{d}\xi}\, \mathrm{d}\xi, \tag{2.25}$$

$$v(\xi) = \int_0^\xi V\, \mathrm{d}\xi. \tag{2.26}$$

Note that $\mathrm{d}V(\xi)/\mathrm{d}\xi$, $u(\xi)$ and $v(\xi)$ are of the same order as $V(\xi)$, defined in equation (2.21). Therefore, since $\gamma(\hat{z})$ and $\mathrm{d}\gamma(\hat{z})/\mathrm{d}\hat{z}$ are also of the same order, (2.24) indicates that $|V_x| = \mathcal{O}(\delta)|V_z|$. We retrieve the classical property that in a boundary layer, the transverse and streamwise velocities are of different magnitudes. We now turn our attention to the vertical momentum equation. Its advection terms are

$$V_x\frac{\partial V_z}{\partial x} = \left[u(\xi)\frac{\mathrm{d}\delta}{\mathrm{d}\hat{z}}\gamma(\hat{z}) - v(\xi)\delta\frac{\mathrm{d}\gamma}{\mathrm{d}\hat{z}}\right]\frac{\partial V(\xi)}{\partial \xi}\frac{\gamma(\hat{z})}{\delta Z_0}, \tag{2.27}$$

$$V_z\frac{\partial V_z}{\partial z} = \frac{V(\xi)\gamma(\hat{z})}{\delta Z_0}\left[\delta V\frac{\mathrm{d}\gamma}{\mathrm{d}\hat{z}} - \xi\frac{\mathrm{d}\delta}{\mathrm{d}\hat{z}}\frac{\mathrm{d}V(\xi)}{\mathrm{d}\xi}\gamma\right]. \tag{2.28}$$

The terms have to be compared with the diffusion term, the leading order of which is easily established as

$$\nu\Delta V_z = \frac{\nu}{(\delta Z_0)^2}\frac{\mathrm{d}^2 V}{\mathrm{d}\xi^2}(\xi)\gamma(\hat{z}) + \mathcal{O}\left(\frac{\nu}{Z_0^2}V\gamma\right). \tag{2.29}$$

A comparison between (2.27)–(2.28) and (2.29) leads us to neglect both advection terms compared to diffusion if the following assumptions hold:

$$\left|\delta\frac{\mathrm{d}\delta}{\mathrm{d}\hat{z}}\gamma\right| Z_0 \left|V\frac{\mathrm{d}V}{\mathrm{d}\xi}\right| \ll \nu\frac{\mathrm{d}^2V}{\mathrm{d}\xi^2}, \quad \left|\delta^2\frac{\mathrm{d}\gamma}{\mathrm{d}\hat{z}}\right| Z_0 \left|V^2\right| \ll \nu\frac{\mathrm{d}^2V}{\mathrm{d}\xi^2}. \tag{2.30}$$

These hypotheses will be checked with respect to the final result. This corresponds to the fact – often met in convection with moderate or large Prandtl number – that the convection boundary layer is established to compensate buoyancy by viscous effects.

Expressions (2.20)–(2.22) are now incorporated into the vertical-momentum conservation law of the steady Boussinesq equations. Keeping the lowest-order terms in δ, we obtain the following ordinary differential equation:

$$\frac{\nu}{\alpha g Z_0^2}\frac{1}{\theta(\xi)}\frac{\mathrm{d}^2V}{\mathrm{d}\xi^2} = -C_1 = -\delta^2(\hat{z})\frac{\tau(\hat{z})}{\gamma(\hat{z})} \tag{2.31}$$

where C_1 is a positive dimensionless constant. As for the heat equation, we establish the following similar estimates for the advection terms:

$$V_x\frac{\partial T}{\partial x} = \left[u(\xi)\frac{\mathrm{d}\delta}{\mathrm{d}\hat{z}}\gamma(\hat{z}) - v(\xi)\delta\frac{\partial\gamma}{\partial\hat{z}}\right]\frac{\mathrm{d}\theta(\xi)}{\mathrm{d}\xi}\frac{\tau(\hat{z})}{Z_0\delta}, \tag{2.32}$$

$$V_z\frac{\partial T}{\partial z} = \frac{V(\xi)\gamma(\hat{z})}{Z_0}\left[\frac{Z_0\Psi_0}{\lambda}\frac{\mathrm{d}T_s}{\mathrm{d}\hat{z}} + \frac{1}{\delta}\left(\theta\delta\frac{\mathrm{d}\tau}{\mathrm{d}\hat{z}} - \xi\frac{\mathrm{d}\delta}{\mathrm{d}\hat{z}}\frac{\mathrm{d}\theta}{\mathrm{d}\xi}\tau(\hat{z})\right)\right]. \tag{2.33}$$

The nonlinear terms of heat advection have to be compared with the temperature diffusion terms, the leading order of which is obviously supplied by

$$\kappa\Delta T = \frac{\kappa}{(Z_0\delta)^2}\frac{\mathrm{d}^2\theta}{\mathrm{d}\xi^2}(\xi)\tau(\hat{z}) + \frac{\kappa\Psi_0}{Z_0}\frac{\mathrm{d}^2\hat{T}_s}{\mathrm{d}\hat{z}} + O\left(\frac{\kappa}{Z_0^2}\theta\tau\right). \tag{2.34}$$

At this point, we formulate the following five additional hypotheses of calculation, that have also to be checked against the final result:

$$\left|\frac{1}{\delta}\frac{\mathrm{d}\delta}{\mathrm{d}\hat{z}}\frac{\mathrm{d}\theta}{\mathrm{d}\xi}\tau\right| \ll \frac{\Psi_0 Z_0}{\lambda}\left|\frac{\mathrm{d}\hat{T}_s}{\mathrm{d}\hat{z}}\right|, \quad \left|\theta\frac{\mathrm{d}\tau}{\mathrm{d}\hat{z}}\right| \ll \frac{\Psi_0 Z_0}{\lambda}\left|\frac{\mathrm{d}\hat{T}_s}{\mathrm{d}\hat{z}}\right|, \tag{2.35}$$

$$\frac{\Psi_0 Z_0}{\lambda}\left|\frac{\mathrm{d}^2\hat{T}_s}{\mathrm{d}\hat{z}^2}\right|\delta^2 \ll \left|\frac{\mathrm{d}^2\theta}{\mathrm{d}\xi^2}\tau\right|, \tag{2.36}$$

$$\left|\delta\frac{\mathrm{d}\delta}{\mathrm{d}\hat{z}}\gamma\right| Z_0 \left|V\frac{\mathrm{d}\theta}{\mathrm{d}\xi}\right| \ll \kappa\frac{\mathrm{d}^2\theta}{\mathrm{d}\xi^2}, \quad \left|\delta^2\gamma\frac{\mathrm{d}\tau}{\mathrm{d}\hat{z}}\right| Z_0 \left|V\theta\right| \ll \kappa\frac{\mathrm{d}^2\theta}{\mathrm{d}\xi^2}. \tag{2.37}$$

The two hypotheses (2.35) allow us to keep the stratification gradient as the leading order of temperature gradient, while assumption (2.36) leads us to neglect vertical heat conduction with respect to horizontal conduction in the convection layer. The last two assumptions (2.37) permit us to neglect two additional advection terms. Consequently, if the five hypotheses (2.35)–(2.37) hold (see the discussion at the end of the present section), we reduce the heat equation to the following second-order ordinary differential equation:

$$\frac{\mathrm{d}\hat{T}_s(\hat{z})}{\mathrm{d}\hat{z}}\delta^2\frac{\gamma(\hat{z})}{\tau(\hat{z})} = C_2 = \frac{\kappa\lambda}{\Psi_0 Z_0^2}\frac{1}{V(\xi)}\frac{\mathrm{d}^2\theta(\xi)}{\mathrm{d}\xi^2} \tag{2.38}$$

where C_2 is a dimensionless constant. Then, from equations (2.31) and (2.38) we easily derive the following fourth-order differential equation for $V(\xi)$

$$V^{(4)} + 4\beta^4 V = 0 \tag{2.39}$$

where β is the dimensionless constant

$$\beta = \frac{1}{\sqrt{2}}[C_1 C_2 Ra_S]^{1/4} = \frac{1}{\sqrt{2}}\delta(\hat{z})\left[\frac{\mathrm{d}\hat{T}_s}{\mathrm{d}\hat{z}} Ra_S\right]^{1/4} \tag{2.40}$$

and Ra_S, the Rayleigh number relative to nonlinear stratification, is defined as

$$Ra_S = \frac{\alpha g \Psi_0 Z_0^4}{\kappa \nu \lambda}. \tag{2.41}$$

The general bounded solution of (2.39) with zero value at $\xi = 0$ is

$$V(\xi) = V_0\, \mathrm{e}^{-\beta\xi} \sin\beta\xi \tag{2.42}$$

and yields the temperature field

$$\theta(\xi) = \theta_0\, \mathrm{e}^{-\beta\xi} \cos\beta\xi \tag{2.43}$$

with the following relationship between the amplitudes:

$$\theta_0 / V_0 = C_2 \Psi_0 Z_0^2 / \left(2\kappa\lambda\beta^2\right) = 2\beta^2 \nu / \left(C_1 \alpha g Z_0^2\right). \tag{2.44}$$

Expression (2.43) has to satisfy the boundary condition corresponding to a fixed heat flux at $x = 0$, i.e.

$$-\frac{\lambda\tau(\hat{z})}{Z_0\delta}\frac{\partial\theta}{\partial\xi}\bigg|_{\xi=0} = \phi_0. \tag{2.45}$$

We hence obtain from (2.43) and (2.40)

$$\theta_0\tau(\hat{z}) = \frac{Z_0\phi_0}{\lambda}\frac{\delta}{\beta} = \sqrt{2}\frac{Z_0\phi_0}{\lambda}\left[\frac{\mathrm{d}\hat{T}_s}{\mathrm{d}\hat{z}} Ra_S\right]^{-1/4} \tag{2.46}$$

and from (2.38)

$$V_0\gamma(\hat{z}) = \frac{\sqrt{2}\kappa}{Z_0}\frac{\phi_0}{\Psi_0} Ra_S^{1/4}\left[\frac{\mathrm{d}\hat{T}_s}{\mathrm{d}\hat{z}}\right]^{-3/4}. \tag{2.47}$$

Coming back to dimensional quantities, orders of magnitude Ψ_0 and Z_0 disappear in (2.46) and (2.47), and the result is

$$\theta_0\tau(\hat{z}) = \left(\frac{\phi_0}{\lambda T_s'}\right)^{1/4}\left(\frac{4\nu\kappa\phi_0^3}{\lambda^3\alpha g}\right)^{1/4}, \tag{2.48}$$

$$V_0\gamma(\hat{z}) = \left(\frac{\phi_0}{\lambda T_s'}\right)^{3/4}\left(\frac{4\alpha g\kappa^3\phi_0}{\nu\lambda}\right)^{1/4}. \tag{2.49}$$

Note the close similarity with (2.14) and (2.15). It remains to supply the expression of $\beta\xi$ as a function of the primitive variables. From (2.40) we easily establish that

$$\beta\xi = \frac{x}{l(z)} \tag{2.50}$$

with

$$l(z) = \left(\frac{4\kappa\nu}{\alpha g T_s'}\right)^{1/4}. \tag{2.51}$$

We remark that the convection boundary layer now has a varying thickness, the form of which can easily be connected with (2.11).

To summarize the results of the present analysis, we may write the approximate solution as

$$T(x,z) = T_s(z) + \left(\frac{\phi_0}{\lambda T_s'(z)}\right)^{1/4}\left(\frac{4\nu\kappa\phi_0^3}{\lambda^3\alpha g}\right)^{1/4}\exp(-x/l(z))\cos(x/l(z)), \tag{2.52}$$

$$V_z(x,z) = \left(\frac{\phi_0}{\lambda T_s'(z)}\right)^{3/4}\left(\frac{4\alpha g\kappa^3\phi_0}{\nu\lambda}\right)^{1/4}\exp(-x/l(z))\sin(x/l(z)). \tag{2.53}$$

By setting $T_s'(z) = \psi_0/\lambda$, we recover the Prandtl solution (2.7)–(2.8) complemented with expressions (2.11), (2.14) and (2.15). To complete this analysis, we now discuss the hypotheses formulated during our derivation. We first note that expressions (2.52) and (2.53) have the same dependence on z as that of $\mathrm{d}T_s(z)/\mathrm{d}z$. Second, we observe that δ, the small parameter related to the boundary layer thickness, behaves like $l(z)/Z_0$ or like $Ra_S^{-1/4}$, the Rayleigh number of nonlinear stratification as defined in (2.41). In other words, our expansion in δ is valid when Ra_S is large. This general feature can be more directly confirmed by inspecting the respective magnitudes of the differential quantities. Thus, taking account of the final results (2.53), a straightforward calculation shows that conditions (2.30) are valid if $Ra_S^{-1/4} \ll Pr$ with $Pr = \nu/\kappa$. On the other hand, the same procedure regarding conditions (2.35) and (2.37) supplies the validity condition $Ra_S^{-1/4} \ll 1$. Assumption (2.36) can be rewritten as $Ra_S^{-1/4} \ll \phi_0/\Psi_0$. These conditions show that a large Rayleigh number of nonlinear stratification is required to ensure accuracy of the results. To sum up, three conditions of validity are required, which can be written in the following compact form:

$$Ra_S^{-1/4} \ll \min\left\{1,\, Pr,\, \frac{\phi_0}{\Psi_0}\right\}. \tag{2.54}$$

These conditions are consistent with the exactness of the Prandtl solution. Namely, when the stratification becomes linear, Z_0 tends to infinity, as does Ra_S. Consequently, our approximate solution (2.52) and (2.53) tends continuously towards the exact solution. The present analytical solution also has two important characteristics of free convection in a stratified medium (see Tanny & Cohen 1998): flow reversal and temperature defect.

3. Application to a storage tank of liquefied gas

Our purpose is now to show that nonlinear stratification can occur in practice, and that our theory may be successfully applied to such a situation. The practical configuration that we consider is liquefied gas storage in a cylindrical tank. The cylinder is filled with a pure substance (e.g. hydrogen), and at its bottom is a thin liquid layer of the substance. The motion in the liquid layer is assumed to be negligible to focus on the natural convection arising in the vapour. Therefore, the tank is assumed to contain a unique gaseous species, the Prandtl number of which is $Pr = 0.71$. The part played by the liquid phase is restricted to maintaining the vapour at a given temperature at $z = 0$, the cylinder bottom (i.e. the liquid–vapour interface). R is the cylinder radius, H is the height of the zone occupied by the

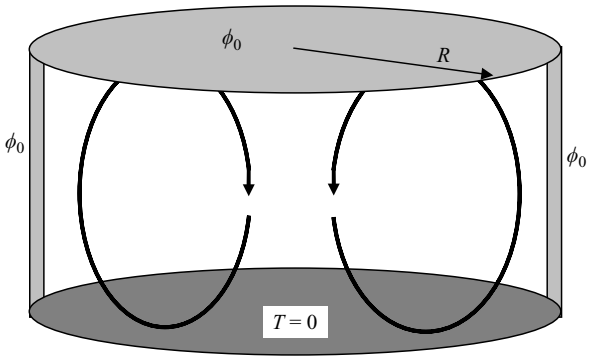

FIGURE 1. Sketch of the vapour part in a liquefied gas storage tank containing a thin liquid layer at the bottom. $10^7 \leqslant R_a \equiv g\alpha\phi_0 R^4/\nu\kappa\lambda \leqslant 10^{12}$; $P_r \equiv \nu/\kappa = 0.71$; $0.25 \leqslant A \equiv H/R \leqslant 1$. g, gravity acceleration; α, thermal expansion coefficient; ϕ_0, imposed uniform flux; ν, kinematic viscosity; κ, thermal diffusivity; λ, heat conductivity.

vapour phase, and $A = H/R$ is the aspect ratio of the vapour zone. We study three values of A ($A = 0.25$, 0.5 and 1) with a particular interest in the practical case $A = 0.25$, although this aspect ratio is less easy to apply the theory, since – as mentioned below – the convective boundary layer is less developed for $A = 0.25$. The thermal boundary conditions are modelled as follows: the vapour cylinder has the liquid–vapour coexistence temperature at its bottom, set to $T_0 = 0$, while at the other cylinder walls the vapour receives ϕ_0, a uniform constant heat flux (an hypothesis that can be expected for a low-temperature storage). The validity of this hypothesis depends on the magnitude of the vapour temperature variations at the walls. We additionally neglect the gas flow rate resulting from vaporization. In the concluding discussion, we shall link both assumptions to two conditions of good insulation that the storage has to fulfil.

A sketch of the system studied is presented in figure 1 where the parameters of the configuration are illustrated. The natural convection is assumed to satisfy the Boussinesq approximations. Note that the Boussinesq equations in a cryogenic system (especially with hydrogen) correspond to a quite demanding approximation, because it requires, among other things, that all temperature variations in the cavity be small compared with the mean absolute temperature.

We are interested in high-Rayleigh-number convection, and we focus on steady axisymmetric flows, for which our theory can operate. The following time-dependent approach will find steady flows up to very high Rayleigh numbers. These flows are hence found stable with respect to two-dimensional perturbations, but a stability study for three-dimensional perturbations was not carried out in the present work; this remains to be checked in future work, because if three-dimensionality should occur, it might drastically restrict the application domain (in the high Rayleigh numbers) of our theory. Therefore, for the time being, we simply state: if a stable axisymmetric solution exists at high Rayleigh number in the tank, the analytical expressions (2.51)–(2.53) then supply acceptable predictions of the flow. Finally, note that the vaporization from the liquid layer at steady state extracts from the vapour the latent heat flux that exactly equilibrates the heat flux received from outside.

3.1. *Mathematical formulation and numerical procedure*

The coupling between the vapour dynamics and the thermal state is now solved within the framework of the unsteady Boussinesq equations. Let Ω_c be the cavity

domain and $\Gamma = \Gamma_+ \cup \Gamma_-$, its boundary; Γ_+ stands for the lateral wall ($r = R$) plus the top wall $z = H$, and Γ_- corresponds to the liquid/vapour interface at $z = 0$. In accordance with our axisymmetrical assumptions, we denote the cylindrical directions $(\boldsymbol{e}_r, \boldsymbol{e}_z)$ respectively the radial and vertical directions. The variables used for non-dimensionalization are the cylinder radius R and the time scale R^2/κ, where κ is the thermal diffusion coefficient. The temperature (i.e. the departure from bottom temperature) is normalized by $R\phi_0/\lambda$, where λ is the thermal conductivity. Pressure and velocities are then normalized with suitable combinations of space–time and weight units (the latter is derived from ρ_0, the fluid mean density). Under these standard conventions, the non-dimensional parameters are the Prandtl and cavity Rayleigh numbers, $Pr = \nu/\kappa$ and $Ra = (g\alpha\phi_0 R^4)/(\nu\kappa\lambda)$, respectively.

In the resulting non-dimensional domain $\Omega_c =]0, 1] \times [0, A]$, we now have the following set of reduced equations:

$$\nabla \cdot \boldsymbol{V} = 0 \qquad \text{in} \quad \Omega_c, \tag{3.1}$$

$$\frac{\partial \boldsymbol{V}}{\partial t} + \nabla \boldsymbol{V} \cdot \boldsymbol{V} = -\nabla \left(\frac{P}{\rho_0} \right) + Pr\,\Delta \boldsymbol{V} + Pr\,Ra\,T\,\boldsymbol{e}_z \qquad \text{in} \quad \Omega_c, \tag{3.2}$$

$$\frac{\partial T}{\partial t} + \nabla T \cdot \boldsymbol{V} = \Delta T \qquad \text{in} \quad \Omega_c, \tag{3.3}$$

with the associated boundary conditions

$$\boldsymbol{V} = 0 \quad \text{on} \quad \Gamma = \Gamma_- \cup \Gamma_+, \tag{3.4}$$

$$T = 0 \quad \text{on} \quad \Gamma_- \quad \text{and} \quad \frac{\partial T}{\partial n} = 1 \quad \text{on} \quad \Gamma_+, \tag{3.5}$$

where $\boldsymbol{V}$ denotes the non-dimensional velocity, T the non-dimensional temperature departure from the temperature of liquid/vapour equilibrium, and P the non-dimensional pressure departure from the hydrostatic pressure of a medium with density unity.

For the initial conditions, the computation is as follows. For the first run, the computation is performed with a relatively small Rayleigh number (say, $Ra = 10^3$), while the fluid is initially assumed to be at rest and the temperature is set to zero. Time integration is performed until steady state is reached. All the solutions we consider here are stationary (e.g. steady states are obtained up to $Ra = 10^{12}$ for $A = 0.25$). Then, the subsequent computations are performed with regularly increasing Ra. Each computation uses the previous (steady) solution as the initial condition.

The numerical computation of system (3.1)–(3.5) requires a precise description of the convective boundary layer. At high Rayleigh number, however, it corresponds to a small length scale (the buoyancy layer thickness). Hence, the numerical method selected is of a spectral-type in space, and developed for the cylindrical geometry. A semi-implicit time discretization of second-order time accuracy is used; it corresponds to the second-order backward implicit Euler scheme, associated with an explicit Adams–Bashforth scheme for the nonlinear terms, and an implicit treatment for the viscous and diffusive terms. At each new discretized time $t^{n+1} = (n+1)\Delta t$ (Δt being the time step), we solve successively a Helmholtz elliptic problem for the temperature and the following generalized Stokes problem for velocity and pressure:

$$\nabla \cdot \boldsymbol{V}^{n+1} = 0 \qquad \text{in} \quad \overline{\Omega}_c, \tag{3.6}$$

$$-Pr\,(\Delta \boldsymbol{V})^{n+1} + \left(\frac{3\boldsymbol{V}}{2\Delta t} \right)^{n+1} + \nabla P^{n+1} = \boldsymbol{S}_V^{n,n-1} \quad \text{in} \quad \Omega_c, \tag{3.7}$$

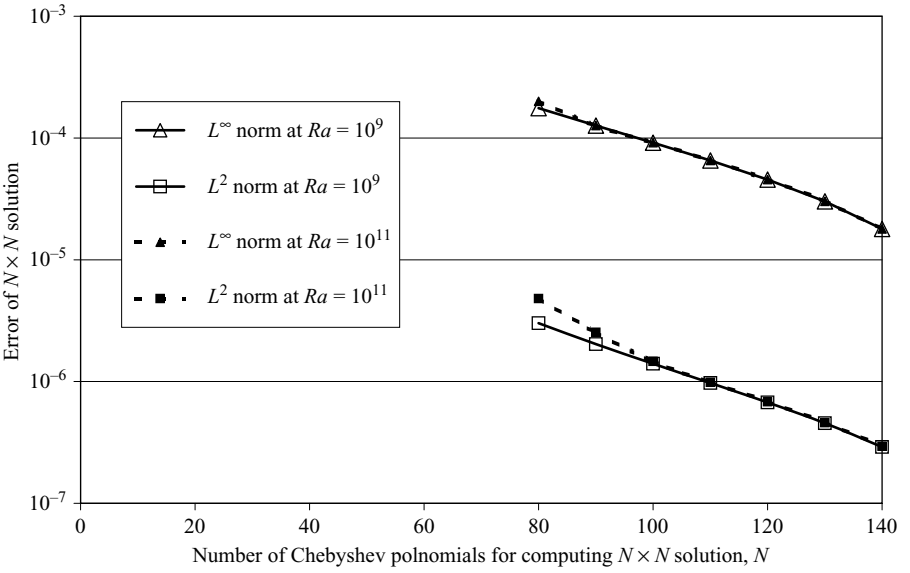

FIGURE 2. Illustration of the spectral exponential convergence of numerical errors, expressed as L^∞ and L^2 norms. For an $N \times N$ Chebyshev expansion, the errors are computed with respect to the solution with $N = 160$, and are plotted versus N.

where $\overline{\Omega}_c$ denotes the closure of Ω_c, and $\boldsymbol{S}_V^{n,n-1}$ is the source term which only depends on quantities already known at previous time steps. This problem is associated with no-slip boundary conditions on Γ.

To solve this problem with a high spatial accuracy, we use a Chebyshev–Chebyshev collocation method in cylindrical geometry such as developed by Le Marec, Guerin & Haldenwang (1996) for both two- and three-dimensional cases. Such a technique has long been known (see e.g. Gottlieb & Orszag 1977, Canuto *et al.* 1988 and Peyret 2002), to provide an exponentially decreasing error in space, once the exact solution is highly regular. Although the pressure treatment in the three-dimensional version of our approach uses a preconditioned Uzawa algorithm, cf. Garba & Haldenwang (2003), the present two-dimensional version uses the influence matrix technique, as described in Le Quéré & Alziary de Roquefort (1985) and Forestier *et al.* (2000), which appeared to be more suitable here (albeit restricted to two-dimensional computations). Subsequent elliptic sub-problems are solved using the partial diagonalization technique, as proposed in Haldenwang *et al.* (1984).

Regarding the precision we achieved, the accuracy of the steady solutions is checked as follows. Let us denote by $T_{M,N}$, the numerical temperature field computed using M [resp. N] Chebyshev polynomials in the radial [resp. vertical] direction. The computations were conducted for two sets of parameters, representative of the range of parameters studied: ($Ra = 10^9$, $A = 0.25$) and ($Ra = 10^{11}$, $A = 0.25$). In both cases, a reference solution has been computed with a large expansion in Chebyshev polynomials (say, $N = M = 160$). For less accurate expansions, the error with respect to the reference solution is then calculated in two norms: the L^2 norm, defined as $\{\int_{\Omega_c} \left(T_{N,N} - T_{160,160}\right)^2 2\pi r \mathrm{d}r\mathrm{d}z\}^{1/2}$, and the L^∞ norm, defined as Max $\mid T_{N,N} - T_{160,160} \mid$ in Ω_c. For both sets of parameters, the error norms have been plotted in figure 2 as a function of N, the number of Chebyshev polynomials selected in both directions. We observe that the regime of exponential convergence is achieved for both solutions. This

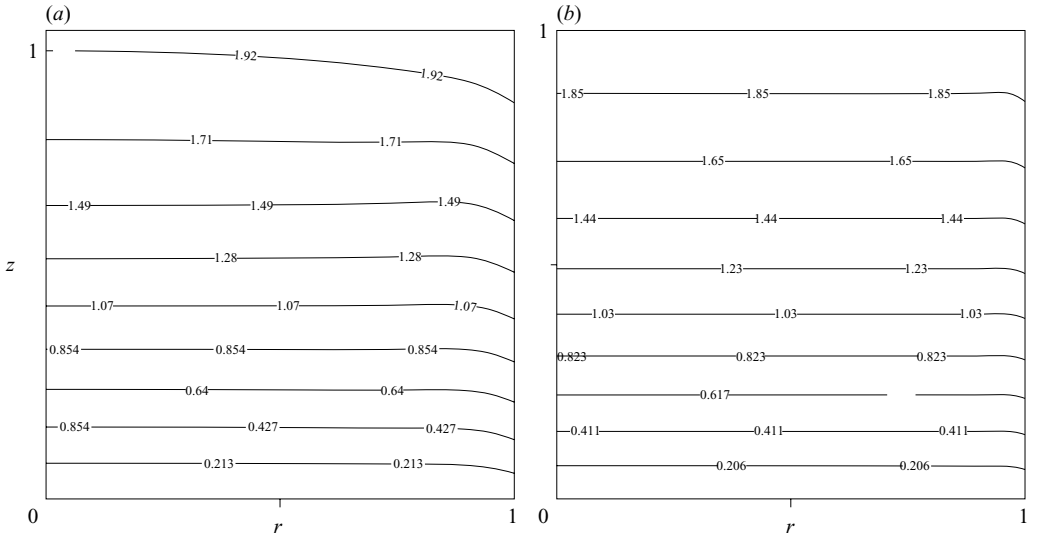

FIGURE 3. Isotherms for $A = 1$ with (*a*) $Ra = 10^3$ and (*b*) $Ra = 10^7$; temperature is normalized with $\phi_0 R/\lambda$.

indicates that all physical length scales are accurately resolved (see e.g. Gottlieb & Orszag 1977 and Canuto *et al.* 1988). Note in figure 2 that the L^2 norm (being an integrated quantity) indicates an error about two decade more accurate than the L^∞ norm, while the precision is independent of Ra when the regime of exponential convergence is attained. In practice, we chose the double Chebyshev expansion large enough to obtain a 4-digit point-wise precision in the range studied: for instance, this accuracy is achieved with $M = 130$ and $N = 120$ for the particular case ($Ra = 10^{11}$, $A = 0.25$), while the time integration uses the time step $\Delta t = 5 \times 10^{-7}$.

3.2. *Qualitative description of the convection in the tank*

The Prandtl number is set to $Pr = 0.71$; the numerical study is conducted with respect to the two other parameters. More precisely, we present results for three different aspect ratios: $A = 1$, $A = 0.5$ and $A = 0.25$; the upper bound on the Rayleigh number can be chosen as large as $Ra = 10^{12}$ for $A = 0.25$. For large enough Rayleigh numbers, a thermal boundary layer develops along the lateral wall, and it becomes thinner as Ra increases. This is clearly observed in figures 3(*a*) and 3(*b*), which plot the isotherms at $Ra = 10^3$ and $Ra = 10^7$ respectively, for $A = 1$. Both figures exhibit a certain amount of stratification of the bulk. Furthermore, we observe in figure 3(*b*) the nonlinearity of the stratification: the isotherms, which correspond to regularly distributed temperatures, are not equally spaced in the cavity.

Further inspection of the tank's thermal state for various pairs of parameters indicates that the maximum temperature of the vapour in the tank decreases with increasing Rayleigh number. This maximum temperature seems to tend at very high Ra to the asymptotic reduced value $A(1 + A)$, as indicated in figure 4, where T_{Max}, the maximum temperature found in the cavity, is plotted with respect to Rayleigh number for different tank aspect ratios. We now turn to the characteristics of the stationary motion. Figure 5 presents the streamlines for three aspect ratios $A = 0.25, 0.5$ and 1, the Rayleigh number being set to $Ra = 10^7$. The streamline patterns indicate that the ascending flow is localized in a vertical boundary layer close to the lateral wall, where we have previously observed the deviation from stratification in figure 3. Both

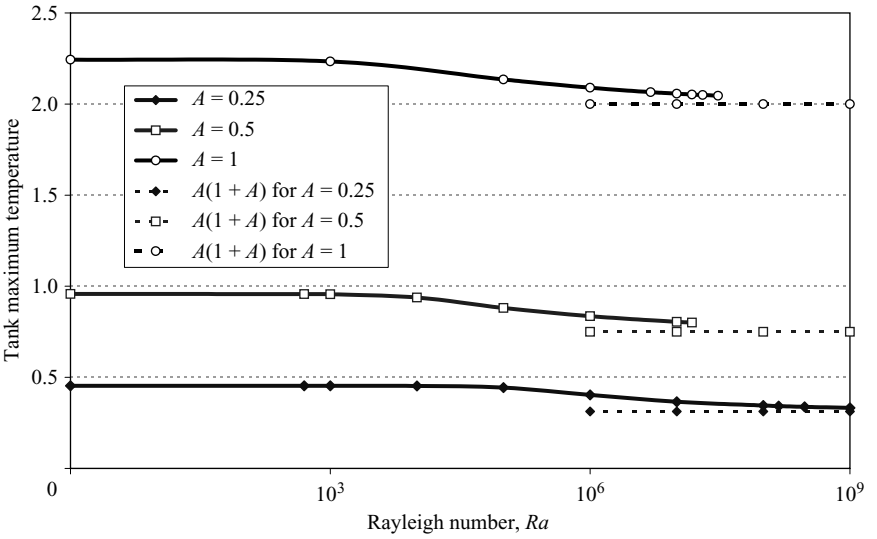

FIGURE 4. T_{Max} vs. Ra for various aspect ratios; horizontal lines correspond to $A(1 + A)$, an heuristically guessed asymptotic value; temperature is normalized with $\phi_0 R/\lambda$.

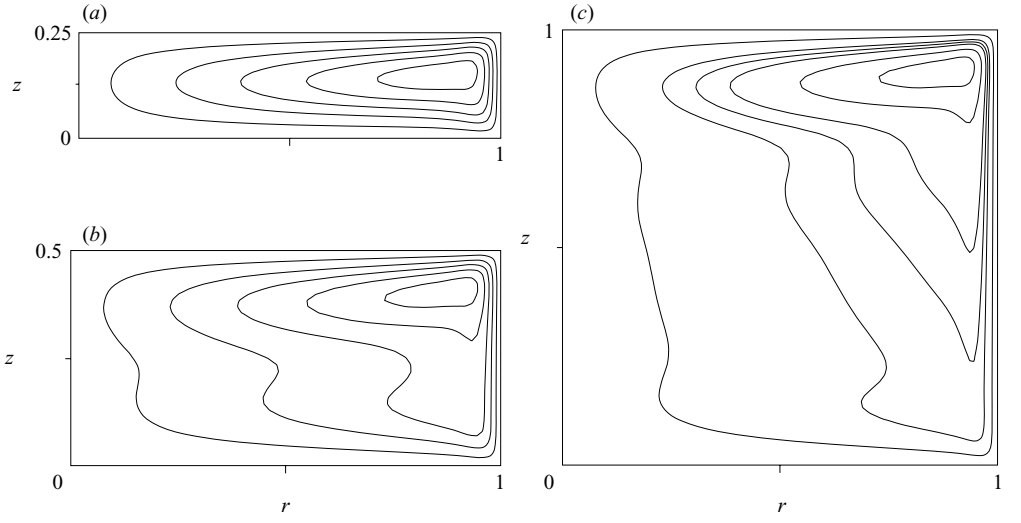

FIGURE 5. Streamlines at $Ra = 10^7$ for aspect ratios (*a*) $A = 0.25$, (*b*) $A = 0.5$ and (*c*) $A = 1$.

thermal (figure 3) and dynamical (figure 5) patterns comprise the convective boundary layer, which has two feed sources: from below and from the bulk, as indicated by the trajectories for $A = 0.5$ and $A = 1$. At $Ra = 10^7$ these general features are not clear for $A = 0.25$, because the convective layer thickness is a length scale not much smaller than the tank height. In this case, an increase in Rayleigh number is needed to ensure a marked separation of the two scales (cavity height and convection layer thickness).

We consider in more detail figure 5(*c*) (i.e. the streamline patterns for $A = 1$) which is representative of the flow field at high values of Ra. On the bottom part of the third and fourth streamlines (starting from the walls), we note a V-shape pattern (this can also be guessed for the second and fifth streamlines in the same figure). This

particular form indicates that – starting from the lateral wall – there is an ascending flow that grows from zero to a maximum, and then decreases until the flow becomes downward. The V-shape pattern is thus the illustration on streamlines of the flow reversal we have mentioned already.

3.3. *Characterization of the bulk nonlinear stratification*

The tank configuration studied here illustrates clearly that high-Rayleigh-number convection induces thermal stratification of the bulk. The present case differs from the situation frequently reported in the literature however, which concerns a linearly stratified medium (i.e. with a uniform vertical temperature gradient). This departure from the standard situation can be explained by the following simple analysis of the energy balance in the tank in steady state.

From the lateral and top surfaces, the tank receives the thermal power $\pi R^2(1+2A)\phi_0$ which exactly supplies the power required by the vaporization at the liquid–vapour interface. If we suppose that heat transfer at the interface is uniform (as suggested by figure 3(*b*) where the stratification seems to reach the interface), we deduce that the thermal flux at the interface is $(1 + 2A)\phi_0$. On the other hand, assuming that stratification is also effective up to the top of the tank, the thermal gradient has to match with ϕ_0/λ. The simplest vertical temperature profile that satisfies both boundary conditions is the quadratic profile, written in non-dimensional form as

$$T_s(z) = (1 + 2A)z - z^2. \tag{3.8}$$

Equation (3.8) results from the simple rationale that the stratification profile has to fit with the non-uniform fluxes that must vertically cross the cavity at high Rayleigh number. On the other hand, the maximum temperature found numerically is located at the top of the cavity and its value is found to be in agreement with this rationale, since equation (3.8) takes the value $A(1+A)$ at $z = A$, which is close to the asymptotic values observed in figure 4. This heuristic approach has to be validated quantitatively by inspecting the numerical data.

We first define $\Omega_B =]0, 0.9] \times [0.1, 0.9A]$ as a sub-domain that excludes a layer along all boundaries. Obviously, Ω_B plays the role of the bulk mentioned in the previous theoretical section. The temperature discrepancy between the bulk numerical temperature field and the one given by equation (3.8) is measured in the $L^\infty(\Omega_B)$ norm [i.e. Max $\mid T(r, z) - T_s(z) \mid$ in Ω_B], and is plotted in figure 6 with respect to Ra for the three values of $A = 0.25$, 0.5 and 1. We observe that all the computed departures from equation (3.8) more or less fit with the curve $0.8Ra^{-1/7}$. As Rayleigh number increases, we note that bulk stratification becomes closer to equation (3.8) and conclude that, for $A = 0.25$, the departure from stratification (3.8) is very weak in the upper range of Rayleigh numbers (say $Ra > 10^9$). The curve $0.8Ra^{-1/7}$ has been obtained by fit of the departures, and for the time being we are unable to propose an explanation for the deviation from stratification. Nevertheless, we are in position to claim that the fluid bulk has the nonlinear stratification given in (3.8) within a precision of a few per cent in the upper range of Rayleigh numbers.

Hence, we can now apply our theory. To anticipate the precision, we have to estimate the value of Ra_S, the Rayleigh number of nonlinear stratification, in this application. We compute its expression with respect to the tank parameters. The heat flux that crosses the stratified bulk varies between ϕ_0 and $(1+2A)\phi_0$. We choose $\Psi_0 = (1+A)\phi_0$ as its order of magnitude. The second derivative of the stratified temperature field equals $-2\phi_0/(\lambda R)$ from equation (3.8). Hence the typical length scale of nonlinear stratification can be set to $Z_0 = R(1 + A)/2$. Consequently, we obtain the following

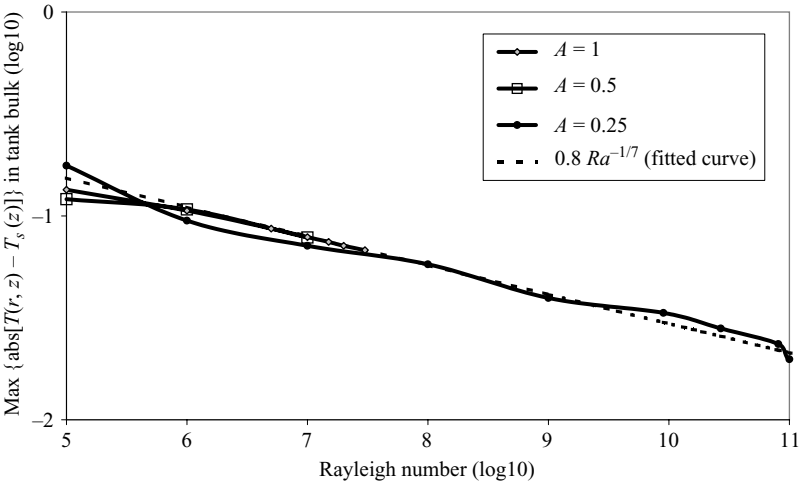

FIGURE 6. Temperature discrepancy in the tank bulk between numerical results and $T_s(z)$ vs. Ra for various aspect ratios A; the dotted line corresponds to $0.8Ra^{-1/7}$.

relationship between Ra_S and Ra:

$$Ra_S = 2Ra\left(\frac{1+A}{2}\right)^5. \tag{3.9}$$

Since Ra_S is proportional to Ra, we can expect a satisfactory application of our theory for high-Ra convection. We nonetheless note that the vertical tank wall is not infinite, and therefore some discrepancies between the numerical and analytical approaches should arise due to the following features: (*a*) the vertical velocity vanishes at both vertical ends of the boundary layer, and (*b*) the flow enters the convective layer with an inlet transverse pattern different from that of a convective layer. Despite these disparities, we nevertheless observe numerous common properties between numerical and analytical predictions.

3.4. *Comparison between theory and numerical simulation*

Using the tank parameters in equations (2.52) and (2.53), we rewrite the theoretical solution with respect to the variables describing the tank, and obtain

$$T(r,z) = (1+2A)z - z^2 + \frac{\cos[(1-r)/l(z)]e^{-[(1-r)/l(z)]}}{[1+2A-2z]^{1/4}}\frac{\sqrt{2}}{Ra^{1/4}}, \tag{3.10}$$

$$V_z(r,z) = \sqrt{2}\frac{\sin[(1-r)/l(z)]e^{-[(1-r)/l(z)]}}{[1+2A-2z]^{3/4}}Ra^{1/4}, \tag{3.11}$$

with

$$l(z) = \sqrt{2}[1+2A-2z]^{-1/4}Ra^{-1/4}. \tag{3.12}$$

In equation (3.12) we note that the boundary layer thickness $l(z)$ is an increasing function of z. We recall that solution (3.10)–(3.11) describes the flow in the vicinity of the lateral wall and is based on the validity of assumptions (2.54) for Ra_S. Since here $\phi_0/\Psi_0 = O(1)$, the three conditions (2.54) roughly reduce to $Ra^{-1/4} \ll 1$. We now carry out a comparison between numerical simulations and analytical approach (3.10)–(3.11) for several sensitive values.

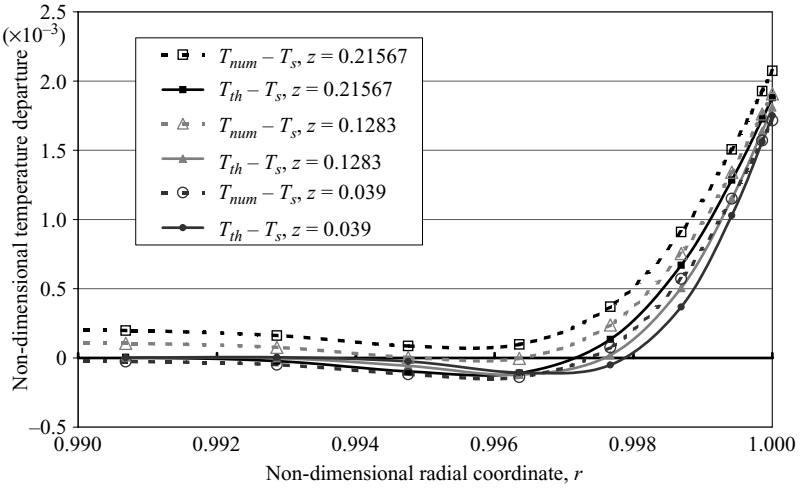

FIGURE 7. Radial profiles of temperature departure from stratification $T_s(z)$ at various vertical coordinates; solid curves correspond to the analytical solution, and dotted curves to the numerical simulation ($A = 0.25$ and $Ra = 3 \times 10^{11}$); temperature is normalized with $\phi_0 R/\lambda$.

With respect to the thermal field, we are faced with the following difficulty: the numerical bulk temperature converges slowly (i.e. as $Ra^{-1/7}$) to the stratification, while the thermal departure from stratification on the wall decreases as $Ra^{-1/4}$. Therefore, we run the risk that the numerical thermal departure from stratification could be disturbed.

The comparison first concerns the radial dependence of the two solutions: we consider the radial profile of the temperature departure from thermal stratification, as well as the radial profile of the ascending velocity. We then study the vertical profiles of the two quantitie $T_m(z)$ and $V_m(z)$ which are, respectively, the thermal departure along the lateral wall (where the radial profile of thermal departure is maximum) and the maximum of the radial profile for the ascending velocity. Both vertical profiles have in turn a maximum, which is localized in the vicinity of the cylinder ceiling (i.e. for $z = A$). Then we compare their values predicted both numerically and analytically. Most comparisons are for high Rayleigh number, say $Ra = 3 \times 10^{11}$, and with $A = 0.25$.

3.4.1. *Comparing the radial profiles*

We focus first on the thermal departures from stratification with respect to the radial temperature profiles. Figure 7 illustrates the temperature deviations from the theoretical stratification T_s at three different vertical positions (i.e. bottom, mid and top positions) in the vicinity of the buoyancy layer (i.e. close to the vertical wall). The numerical data correspond to the dotted curves. In all cases, numerical and analytical solutions agree well with respect to the temperature defect close to the wall: the temperature departure from thermal stratification becomes negative just outside the convective boundary layer. However, as can be observed on the left part of the two dotted curves in figure 7, the temperature departure differs from zero in the bulk. In other words, the numerical stratification differs slightly from T_s. This possibility was mentioned above. This weak discrepancy disturbs the departure profile by shifting the numerical temperature field above the analytical one slightly. This feature nonetheless preserves the qualitative agreement between the two approaches: (*a*) the boundary

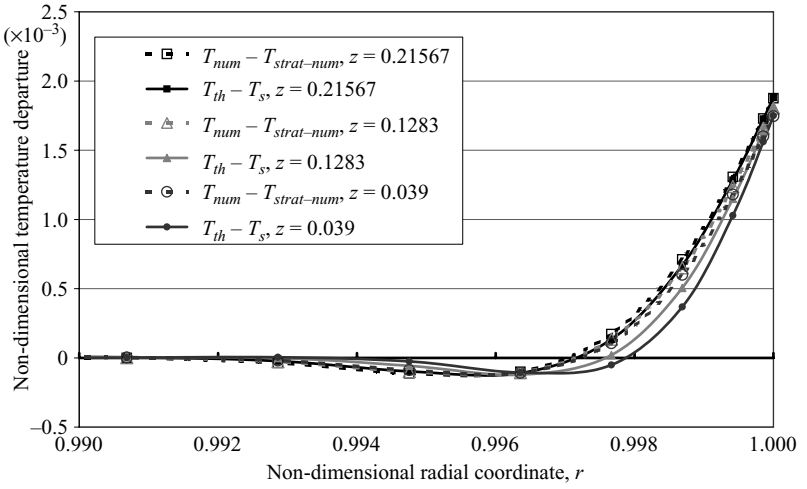

FIGURE 8. Radial profiles of temperature departure from the actual numerical stratification at various vertical coordinates; solid curves correspond to the analytical solution, and dotted curves to the numerical simulation ($A = 0.25$ and $Ra = 3 \times 10^{11}$); temperature is normalized with $\phi_0 R/\lambda$.

layer thickness that results from numerical data increases with z, (b) the temperature departure also increases with the vertical position.

We now alter the definition of the numerical departure profiles to the deviation from the actual numerical stratification in the bulk (instead of $T_s(z)$), and plot in figure 8, which compares the same quantities as in figure 7. We observe that the agreement is very good at the top of the wall, where both numerical and analytical curves almost coincide. At the bottom part of the wall, the agreement is quite poor however, while it is only just satisfactory in the mid position. The reason is undoubtedly the presence of a corner at the wall bottom, and the fact that the flow starts its ascending motion with a thermal profile established previously in a complex boundary layer along the liquid. The latter should tend to exaggerate the thermal layer thickness immediately at the entrance. Quantitatively, we define η, the layer thickness, as $\eta = 2(1 - r_b)$, where r_b is such that $\theta(r = r_b) = \theta(r = 1)/2 = \theta_{max}/2$. We estimate at about 25% the discrepancy in boundary layer thickness at the bottom. This then reduces to 12% at the mid cavity, and to 4% at the top of the layer. Apart from this noticeable discrepancy in thermal layer thickness, a further quantitative comparison between the two approaches is satisfactory: every pair of curves gives the same temperature at the wall, as observed in figure 8.

We turn next to the vertical component of velocity, for which the validation is more easily conducted, because we are now comparing two (numerical and analytical) absolute values. Figure 9 shows the radial profiles of vertical velocity plotted at the same vertical position. The agreement between analytical and numerical profiles is very good, where the convective boundary layer is well established i.e. in the upper half-cylinder. The discrepancy is acceptable in mid cavity. On the other hand, close to the bottom (at $z = 0.039$) the boundary layer thickness from the numerical solution is again too large in comparison with (3.11). This effect corresponds to the upstream conditions which are quite far from the domain of applicability our theory. It is noteworthy that both maxima of velocity at the bottom are nevertheless in close agreement.

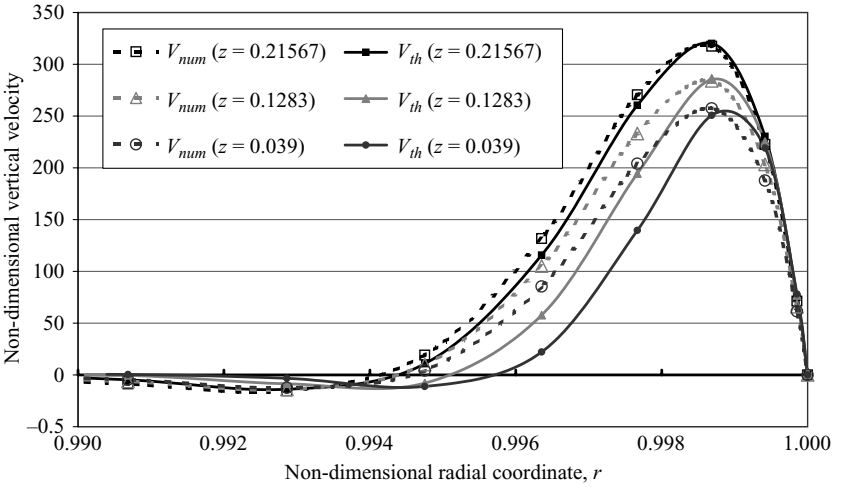

FIGURE 9. Comparison of radial profiles of vertical velocity at three different vertical positions; solid curves correspond to theory, and dotted curves to the numerical computation ($A = 0.25$ and $Ra = 3 \times 10^{11}$); velocity is normalized with κ/R.

To summarize this step of validation with respect to radial profiles, both numerical and analytical approaches yield results that possess the two characteristics of the convection on a vertical plate in a stratified medium: temperature defect and flow reversal. The agreement between numerical and analytical solutions for the radial dependence is excellent in the upper part of the vertical wall, acceptable in mid cavity, and poor at the bottom. The main discrepancy corresponds to a deviation in the convective layer thickness: applying the theory leads to an underestimate of the actual boundary layer thickness with a deviation that depends on the vertical position. An estimate of this discrepancy gives a difference of less than 5% at the top of the layer, 15% at the mid cavity, and about 25% at the bottom, for both thermal and velocity boundary layers. We conclude that the analytical approach supplies an excellent prediction of the radial dependence on the upper part of the wall, but only an acceptable prediction close to the layer entrance.

3.4.2. *Comparison of vertical dependences*

In figure 9, we observe that the maxima of each pair of numerical and analytical curves coincide well. We can therefore expect a good prediction of the overall convection characteristics almost everywhere in the buoyancy layer. We consider the thermal field first. From expression (3.10) we note that at a fixed value of z the tank temperature is maximum at $r = 1$. Furthermore, this maximum increases with z. More precisely, T_m, the maximum (with respect to r) of the temperature departure from stratification T_s equals

$$T_m(z) = T(r = 1, z) - T_s(z) = \frac{\sqrt{2}}{[1 + 2A - 2z]^{1/4} Ra^{1/4}}. \tag{3.13}$$

A comparison between the numerical departure from theoretical stratification T_s and the departure profile given by equation (3.13) is illustrated in figure 10 for $A = 0.25$ and $Ra = 3 \times 10^{11}$. The agreement is quite satisfactory at most vertical positions, except at both ends of the convective layer, where the flow interacts with a horizontal boundary layer at both corners. In view of figure 8, where temperature data on the

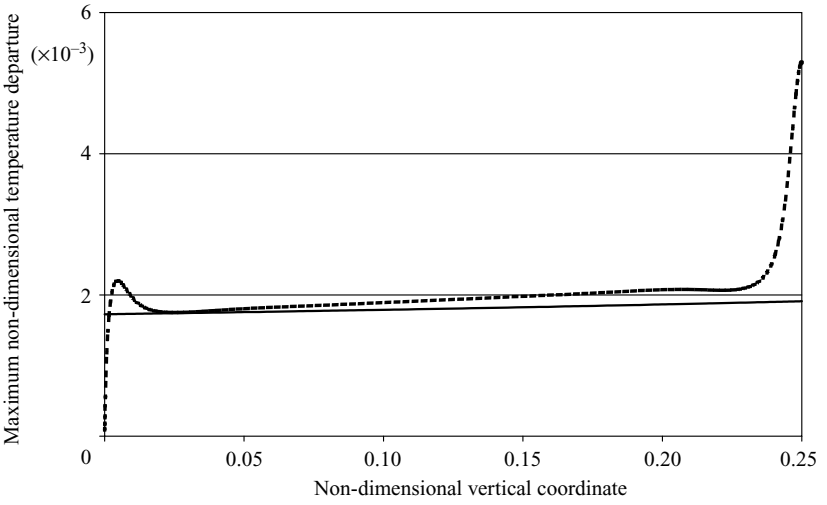

FIGURE 10. Temperature departure from stratification T_s on the tank lateral wall vs. vertical coordinate for $A = 0.25$ and $Ra = 3 \times 10^{11}$: comparison between numerical (dotted) and analytical (solid) predictions.

wall coincide perfectly, we can conclude that the small thermal deviation occurring on the wall in figure 10 is due to a deviation of the numerical stratification from the theoretical one (T_s). A rough estimate indicates that the difference remains lower than 10% in the layer core (i.e. far enough from the corners), though note that the present theory nevertheless supplies an excellent prediction because this discrepancy only concerns a correction. It is furthermore evident that the highest temperature is not attained at the end of the convective layer, because after the upper corner the flow experiences a new heating process in an horizontal thermal layer. For the ascending velocity along the lateral wall, expression (3.11) provides us with the maximum value of each radial profile as follows:

$$V_m(z) = \frac{\mathrm{e}^{-\pi/4}}{[1 + 2A - 2z]^{3/4}} Ra^{1/4}. \tag{3.14}$$

Figure 11 presents a comparison between the analytical results from expression (3.14) and the numerical data computed at $Ra = 3 \times 10^{11}$ and $A = 0.25$. We observe a nearly perfect agreement (difference of the order of 2%) between the two ascending velocities, the close vicinity of both bottom and top cavity corners excepted. This confirms the quality of the present theory and its potential for applications. This result also justifies the need for an extension of the Prandtl theory, because in accordance with the Prandtl theory the latter profile would have been rigorously flat (i.e. independent of z).

3.4.3. *Extreme quantities in the tank*

We denote by V_{Max} the largest ascending velocity predicted by our theory. The locus where this maximum is reached is situated at $z = A$, i.e. at the top of the ascending layer. This is consistent with the numerical prediction, as indicated in figure 11. From expression (3.14)

$$V_{Max} = \mathrm{e}^{-\pi/4} Ra^{1/4}. \tag{3.15}$$

We first observe that this expression is independent of A. This agrees with the numerical data plotted in figure 12, where the overall maxima of the vertical velocity

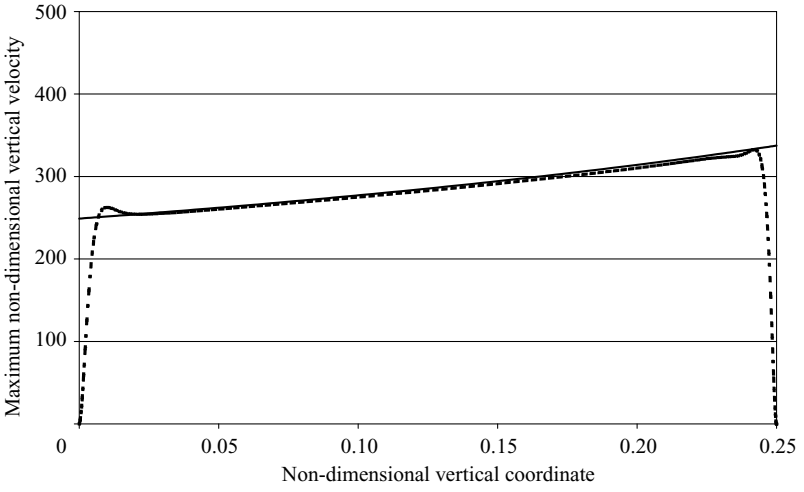

FIGURE 11. Vertical profile of maximum (with respect to radius) ascending velocity (for $Ra = 3 \times 10^{11}$ and $A = 0.25$): comparison between numerical (dotted) and analytical (solid) predictions.

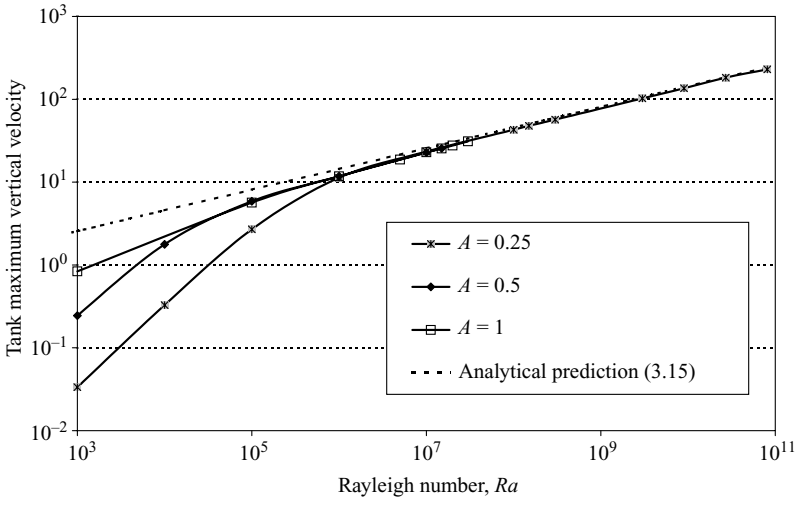

FIGURE 12. Numerical predictions of maximum ascending velocity vs. Rayleigh number for different aspect ratios; velocity is normalized with κ/R. Dotted straight line corresponds to theoretical prediction $e^{-\pi/4} Ra^{1/4}$.

are plotted for various A; the three (plain) curves show the same asymptotic behaviour, which corresponds to an ascending velocity proportional to $Ra^{-1/4}$. Furthermore, fitting these asymptotic numerical results on the maximum ascending velocity, as plotted in figure 12, provides us with the following estimate: $V_{Max} \sim 0.44 Ra^{1/4}$. The fitting constant of 0.44 compares well with $e^{-\pi/4} \approx 0.456$, the theoretical constant in expression (3.15).

We next consider another overall quantity: T_{Max}, the highest temperature in the tank. It is easy to see that theoretical expression (3.10) gives the highest temperature

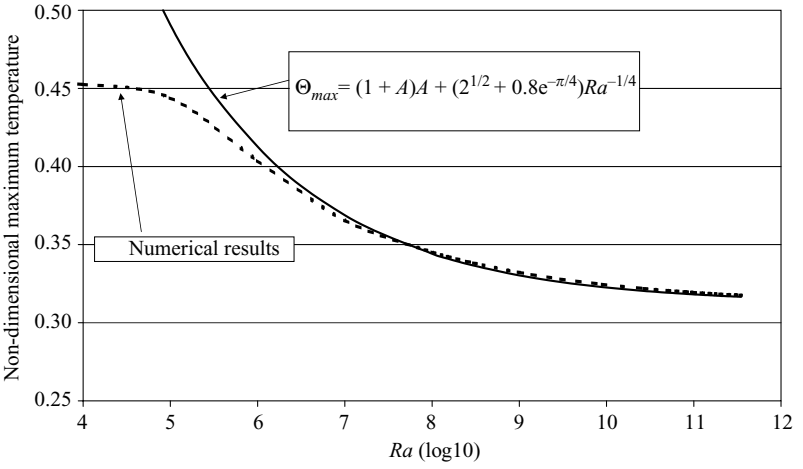

FIGURE 13. Maximum temperature T_{Max} for aspect ratio $A = 0.25$: analytical predictions (from (3.18)), plotted vs. Ra, are compared with numerical results (dotted curve).

for $(r = 1, z = A)$ as

$$T_{Max}^{c.b.l.} = (1 + A)A + \frac{\sqrt{2}}{Ra^{1/4}} \tag{3.16}$$

(where c.b.l. stands for convective boundary layer). Unfortunately, this result cannot predict the actual value of the storage maximum temperature; the tank ceiling continues to heat the vapour. When the fluid passes along the top wall, a second heat transfer across an horizontal thermal layer occurs. This heating process seems to be more complex to interpret, because it is coupled with the return descending flow. Let us denote by $\Delta\Theta$ the additional non-dimensional temperature increase when the fluid flows along the tank ceiling subjected to uniform heating. Thermal boundary layer theory provides us with the classic expression (see e.g. Schlichting 1968)

$$\frac{\phi_0 R}{\lambda}\Delta\Theta = \frac{\phi_0}{\rho c_p U} f\left(\frac{L}{d}\right) \tag{3.17}$$

where $f(L/d)$ is a particular function of the ratio of length to thickness of the layer, and U is the typical velocity. For the present problem, $f(L/d)$ seems impossible to calculate theoretically. Consequently, we turn to a different estimate, which can easily be obtained from our numerical results concerning the tank flow: as the Rayleigh number varies, we remark that the product $V_{Max}\Delta\Theta$ remains more or less constant, of the order of $V_{Max}\Delta\Theta \approx 4/5$. Therefore, the capability of the theory to give V_{Max} (equation (3.15)) allows us to supply an analytical prediction of the overall maximum temperature:

$$T_{Max} = T_{Max}^{c.b.l} + \Delta\Theta = (1 + A)A + \frac{5\sqrt{2} + 4e^{-\pi/4}}{5Ra^{1/4}}. \tag{3.18}$$

To conclude the numerical validation of (3.18), we have plotted in figure 13 the maximum temperature in the storage tank obtained from our computations, as well as the data from equation (3.18), for $A = 0.25$ and the whole range of Rayleigh numbers. The agreement is excellent at large Ra; one can now claim that expression (3.18) supplies the vapour maximum temperature in a storage tank at high Rayleigh number (say $Ra > 10^7$), and consequently the thermal profile of the tank tends to

$T_s(z)$ everywhere as Ra tends to infinity (and as long as the flow remains axisymmetric and steady).

4. Conclusions

This article aimed to derive a new analytical approximate solution for convection in a stratified medium induced by a uniformly heated vertical plate. The stratification is assumed to be nonlinear; the corresponding vertical temperature gradient therefore has an intrinsic length scale of variation. The derivation we have carried out supposes that this length scale is large compared with the intrinsic lengths in the convection boundary layer along the plate. This hypothesis was expressed in the form of conditions (2.54).

We then applied this theory to the practical problem of a liquefied gas storage tank in order to predict the characteristics of the convection flow induced by the external heat transfer through the tank walls. The model of the convection in the cylindrical tank was chosen in the simplest way, and remains to be justified (see below). Under this formulation, the convection flow was numerically computed with a high-precision method. Inspection of our numerical data showed that the flow is nonlinearly stratified in the bulk. This stratification profile has been found to converge slowly towards some quadratic profile, which is then used as an input required in applying the theory.

We obtained several successful comparisons between numerical data and theoretical predictions. In a general manner, the comparison of the ascending velocities is excellent in the upper half of the convection layer. In the lower half, the convection layer thickness is disturbed (within the range of 25%) by the inlet conditions which come from the bottom corner. This upstream perturbation is progressively damped along the convection boundary layer. For the thermal field, we showed that it converges towards the proposed quadratic profile of stratification as the Rayleigh number tends to infinity (as indicated by expressions (3.10) and (3.18)). When attempting to validate the form of the departure from this general profile in the layer (i.e. a first-order correction), we were faced with the difficulty that the discrepancy in the bulk stratification induces a systematic 10% difference between the numerical and analytical departures.

To complete this application of the theory, it remains to analyse the coherence of the present results with both our main hypotheses in convection modelling: the vaporization flow rate is negligible, and the temperature variations in the tank have a little influence on imposed thermal flux boundary conditions. Vaporization flow can be neglected (at the liquid–vapour interface) if its ratio to the typical convective velocity is much smaller than one, i.e. if

$$\frac{(1+2A)\phi_0}{\rho_0 L_{vap}} \ll \left(\frac{\alpha g \phi_0 \kappa^3}{\nu\lambda}\right)^{1/4},$$

L_{vap} being the latent heat. In other words, the assumption holds if the following condition on the imposed heat flux is satisfied:

$$\phi_0 \ll \left[\frac{\rho_0 L_{vap}(\alpha g \kappa^3/\nu\lambda)^{1/4}}{1+2A}\right]^{4/3},$$

which represents a first condition of good insulation that is needed to validate the use of the present model for application to liquefied gas storage (here, good insulation

means that the heat flux, which enters the tank, has to be small compared to a given value).

Regarding the assumption that a uniform thermal flux can be imposed on the upper and lateral boundaries, we have to check that the tank inner temperature fluctuations, as given in equation (3.18), are small compared with the temperature difference between the inside and the outside of the tank, i.e. $T_{max} \ll T_{out}$, where T_{out} stands for the departure of the external temperature from T_0, the liquid/vapour equilibrium temperature. Finally, the second condition of good insulation is

$$\phi_0 \ll \frac{T_{out}\lambda}{A(1+A)R}.$$

Even for practical applications in cryogenic gas storage, the second assumption might be more difficult to fulfil, especially for a tank of large size.

In spite of this last restriction for possible applications, we have shown that our approximate theory is capable of predicting, with a very acceptable precision, the characteristics of a practical case of laminar convection in an enclosure, where a nonlinear stratification occurs at high Rayleigh number.

The authors thank the French National Space Agency (CNES) for the financial support granted within the framework of COMPERE program.

REFERENCES

Baines, W. D. & Turner, J. S. 1969 Turbulent buoyant convection from a source in a confined region. *J. Fluid Mech.* **37**, 51–80.

Canuto, C., Hussaini, Y., Quarteroni, A. & Zang, T. A. 1988 *Spectral Methods in Fluid Dynamics*. Springer.

Forestier, M. Y., Pasquetti, R., Peyret, R. & Sabbah, C. 2000 Spatial development of wakes using a spectral multi-domain method. *Appl. Numer. Math.* **33**, 207–216.

Garba, A. & Haldenwang, P. 2003 Study of preconditioners for collocation Chebyshev approximation of the 2D and 3D Generalized Stokes Problem. *J. Comput. Phys.* **191**, 282–304.

Gill, A. E. 1966 The boundary-layer regime for convection in a rectangular cavity. *J. Fluid Mech.* **26**, 551–537.

Gill, A. E. & Davey, A. 1969 Instabilities of buoyancy driven system. *J. Fluid Mech.* **35**, 775–798.

Gottlieb, D. & Orszag, S. A. 1977 *Numerical Analysis of Spectral Methods: Theory and Applications*. SIAM-CBMS, Philadelphia.

Haldenwang, P. 1986 Unsteady numerical simulation by Chebyshev spectral methods of natural convection at high Rayleigh number. In *Significant Questions in Buoyancy Affected Enclosure or Cavity Flow* (ed. J. A. C. Humphrey *et al.*) ASME/HTD, vol. **60**, pp. 45–51.

Haldenwang, P., Labrosse, G., Abboudi, S. & Deville, M. 1984 Chebyshev 3D spectral and 2D pseudospectral solvers for the Helmholtz equation. *J. Comput. Phys.* **55**, 115–128.

Henkes, R. A. W. M. & Hoogendoorn, C. J. 1989 Laminar natural convection boundary-layer flow along a heated vertical plate in stratified environment. *Intl J. Heat Mass Transfer* **32**, 147–155.

Hunt, G. R., Cooper, P. & Linden, P. F. 2001 Thermal stratification produced by plumes and jets in enclosed spaces. *Building Environ.* **36**, 871–882.

Jaluria, Y. & Gebhart, B. 1974 Stability and transition of buoyancy induced flows in a stratified medium. *J. Fluid Mech.* **66**, 593–612.

Krizhevsky, L., Cohen, J. & Tanny, J. 1996 Convective and absolutes instabilities of a buoyancy induced flow in a thermally stratified medium. *Phys. Fluids* **8**, 971–977.

Kulkarni, K., Jacobs, H. R. & Hwang, J. J. 1987 Similarity solution for natural convection flow over an isothermal vertical wall immersed in thermally stratified medium. *Intl J. Heat Mass Transfer* **30**, 691–698.

Le Marec, C., Guerin, R. & Haldenwang, P. 1996 A Chebyshev collocation method for convective flow induced by unidirectional solidification in a cylinder. *Intl J. Numer. Meth. Fluids* **22**, 393–409.

Le Quéré, P. & Alziary de Roquefort, T. 1985 Computation of natural convection in two-dimensional cavities with Chebyshev polynomials. *J. Comput. Phys* **57**, 210–228.

Peyret, R. 2002 *Spectral Methods for Incompressible Viscous Flow*. Springer.

Prandtl, L. 1952 *Essentials of Fluid Dynamics*. Hafner Publishing Company, New York.

Ravi, M. R., Henkes, R. A. W. M. & Hoogendoorn, C. J. 1994 On the high Rayleigh number structure of steady laminar natural-convection flow in a square enclosure. *J. Fluid Mech.* **262**, 325–351.

Schlichting, H. 1968 *Boundary Layer Theory* 6th Edn. McGraw-Hill.

Shapiro, A. & Fedorovich, E. 2004*a* Prandtl number dependence of unsteady natural convection along a vertical plate in a stably stratified fluid. *Intl J. Heat Mass Transfer* **47**, 4911–4927.

Shapiro, A. & Fedorovich, E. 2004*b* Unsteady convectively driven flow along a vertical plate immersed in a stably stratified fluid. *J. Fluid Mech.* **498**, 333–352.

Sundstrom, L. G. & Kimura, S. 1996 On laminar free convection in inclined rectangular enclosures. *J. Fluid Mech.* **313**, 343–366.

Tanny, J. & Cohen, J. 1998 The mean temperature field of a buoyancy-induced boundary layer adjacent to a verticale plate immersed in a stratified medium. *Intl J. Heat Mass Transfer* **41**, 2125–2130.

Tao, J., Le Quéré, P. & Xin, S. 2004 Spatio-temporal instability of the natural-convection boundary layer in thermally stratified medium. *J. Fluid Mech.* **518**, 363–379.

Turner, J. S. 1973 *Buoyancy Effects in Fluids*. Cambridge University Press.

Yang, K. T., Novotny, J. L. & Cheng, Y. xS. 1972 Laminar free convection from nonisothermal plate immersed in a temperature stratified medium. *Intl J. Heat Mass Transfer* **15**, 1097–1109.